Foam Generation by Capillary Snap-Off in Flow Across a Sharp Permeability Transition

Swej Y. Shah and **Karl-Heinz Wolf,** Delft University of Technology; **Rashidah M. Pilus,** Universiti Teknologi Petronas; and **William R. Rossen,** Delft University of Technology

Summary

Foam reduces gas mobility and can improve sweep efficiency in an enhanced-oil-recovery (EOR) process. Previous studies show that foam can be generated in porous media by exceeding a critical velocity or pressure gradient. This requirement is typically met only near the wellbore, and it is uncertain whether foam can propagate several tens of meters away from wells as the local pressure gradient and superficial velocity decreases. Theoretical studies show that foam can be generated, independent of pressure gradient, during flow across an abrupt increase in permeability. In this study, we validate theoretical predictions through a variety of experimental evidence. Coreflood experiments involving simultaneous injection of gas and surfactant solution at field-like velocities are presented. We use model consolidated porous media made out of sintered glass, with a well-characterized permeability transition in each core. The change in permeability in these artificial cores is analogous to sharp, small-scale heterogeneities, such as laminations and cross laminations. Pressure gradient is measured across several sections of the core to identify foam-generation events and the subsequent propagation of foam. X-ray computed tomography (CT) provides dynamic images of the coreflood with an indication of foam presence through phase saturations. We investigate the effects of the magnitude of permeability contrast on foam generation and mobilization. Experiments demonstrate foam generation during simultaneous flow of gas and surfactant solution across a sharp increase in permeability, at field-like velocities. The experimental observations also validate theoretical predictions of the permeability contrast required for foam generation by "snap-off" to occur at a certain gas fractional flow. Pressure-gradient measurements across different sections of the core indicate the presence or absence of foam and the onset of foam generation at the permeability change. There is no foam present in the system before generation at the boundary. CT measurements help visualize foam generation and propagation in terms of a region of high gas saturation developing at the permeability transition and moving downstream. If coarse foam is formed upstream, then it is transformed into stronger foam at the transition. Significant fluctuations are observed in the pressure gradient across the permeability transition, suggesting intermittent plugging and mobilization of flow there. This is the first CT-assisted experimental study of foam generation by snap-off only, at a sharp permeability increase in a consolidated medium. The results of experiments reported in this paper have important consequences for a foam application in highly heterogeneous or layered formations. Not including the effect of heterogeneities on gas mobility reduction in the presence of surfactant could underestimate the efficiency of the displacement process.

Introduction

Foams are a distribution of discontinuous gas bubbles in a continuous liquid phase. They can be considered as an example of multiphase "condensed soft-matter" systems. Foams have numerous applications in the food and chemical industries and in material science. This work focuses on the application of foam to EOR; more specifically, to capillary-dominated mechanisms of foam generation in porous media. Much of the world's EOR production can be attributed to the injection of gases, especially carbon dioxide (CO_2) and steam. Gas-injection processes, however, are often cursed by unfavorable mobility ratios and differences in fluid densities, which can lead to poor sweep efficiency. In the presence of foam, gas mobility is significantly reduced (Bernard and Holm 1964; Huh and Handy 1989; Rossen 1996), leading to a more "viscosified" gas that gives better sweep efficiency.

There are three main mechanisms of creation of lamellae (liquid films separating bubbles): lamella division, snap-off, and "leave-behind" (Kovscek and Radke 1994; Rossen 1996). Lamella division, as can be inferred from **Fig. 1,** requires that at least one lamella or lens be initially present. Leave-behind primarily occurs during gas invasion through a liquid-filled medium and is more prevalent during a drainage process. Snap-off can occur by several mechanisms (Rossen 2003). One mechanism is Roof snap-off (Ransohoff and Radke 1988), which occurs as gas penetrates a narrow pore throat and drains liquid from a wide pore body, as illustrated in Fig. 1b. Another mechanism is snap-off as gas flows across a sharp increase in permeability (Falls et al. 1988; Rossen 1999; Hirasaki et al. 2000; Li and Rossen 2005; Tanzil et al. 2002). This mechanism is the subject of this paper and is discussed further below.

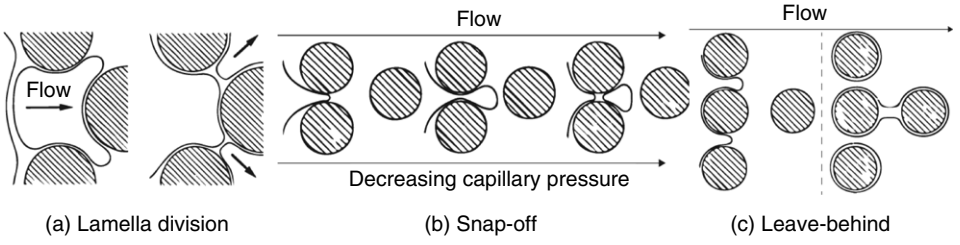

Fig. 1—Mechanisms of lamella creation in porous media (Kovscek and Radke 1994).

Foams can be destroyed either by rupturing of the lamellae (for example, through mechanical disturbances or high capillary pressure) or by gas diffusion from smaller to larger bubbles within a pore because of differences in gas pressure. With respect to flow in porous

This paper (SPE 190210) was accepted for presentation at the SPE Improved Oil Recovery Conference, Tulsa, 14–18 April 2018, and revised for publication. Original manuscript received for review 4 June 2018. Revised manuscript received for review 20 July 2018. Paper peer approved 28 August 2018.

media, foam generation and foam propagation and stability are sensitive to several parameters, including injection rates, local pressure gradient, porosity, permeability, capillary pressure, and oil saturation and composition. Laboratory experiments show that creation of strong foam in steady gas-liquid flow requires exceeding either a minimum velocity ($u^{\min}$) or a minimum pressure gradient, denoted as $\nabla P^{\min}$ (Ransohoff and Radke 1988; Rossen and Gauglitz 1990; Gauglitz et al. 2002). Creation of foam in this case is thought to depend on mobilization of lenses and lamellae and subsequent lamella division. This criterion depends on the experimental procedure followed, and the threshold might be lower for a drainage process (for example, coinjection of gas and surfactant solution into a liquid-saturated core) owing to creation of lamellae by Roof snap-off and leave-behind (Rossen and Gauglitz 1990). Nevertheless, the minimum-velocity or pressure-gradient threshold, as reported in the literature, can be overcome only near a well in a conventional reservoir and is much higher than that encountered away from wells deep inside the formation. This might have unfavorable consequences for foam propagation far from the injection well, as suggested by the experiments of Friedmann et al. (1994) and the modeling of Ashoori et al. (2012), who used the model of Kam (2008), where foam-generation rate is a function of pressure gradient only.

Several studies have indicated, however, that foam can be generated independent of pressure gradient, by snap-off, as gas and liquid flow across a sharp increase in permeability (Falls et al. 1988; Rossen 1999; Hirasaki et al. 2000; Tanzil et al. 2002; Li and Rossen 2005). The extreme case of this phenomenon occurs at the outlet of the core in the form of foam generation as a consequence of the capillary end effect. Yortsos and Chang (1990) presented the solution for steady gas-liquid flow across a permeability jump. Capillary continuity implies an increase in wetting-phase saturation (or reduction in capillary pressure) upstream of the permeability transition (van Lingen 1998), which causes lamella creation by snap-off. In flow from high to low permeability, the opposite is expected to happen. Numerical simulations of two-phase flow from high to low permeability were reported by Chang and Yortsos (1992). The nonwetting phase accumulates at the boundary in the high-permeability zone, similar to gas trapping often witnessed at the entrance of a core during gas-liquid injection. The same mechanism is responsible for the entrapment of oil in highly laminated sandstones as reported in the experiments of van Lingen et al. (1996). To summarize, during gas-liquid flow from high to low permeability, a dried-out zone would exist at the boundary, creating conditions unfavorable for foam generation.

Sharp changes in permeability are quite common in petroleum reservoirs. Structural features that offer this sort of heterogeneity can exist across a large range of length scales. For example, in laminated and cross-laminated sandstones, the size of each unit could typically range from 1 to 1000 cm (Reineck and Singh 1980). Unconformities such as layer boundaries can extend from a few meters to several hundred meters in length. Foam generation can occur as gas migrates upward, because of gravity, across these layer boundaries, in the presence of surfactant solution. Gas and surfactant solution can also be driven to flow across vertical increments in permeability in the near-wellbore region when injected through highly deviated wells. While vertical anisotropy is more ubiquitous, laterally occurring permeability changes are also important as foam-generation sites because of the driving force of pressure gradient in the horizontal direction. Cross laminations offer laterally occurring permeability changes oriented perpendicular or at an incline to the direction of fluid flow. **Fig. 2** shows two of the most-common classifications of crossbed units. As can be seen in the figure, the heterogeneity between consecutive laminae is usually a result of zones with contrasting grain size. Hartkamp-Bakker (1993) measured permeability contrasts in outcrop and reservoir core samples with crossbed laminae and reported contrasts ranging from 1:1 to 27:1 between different units.

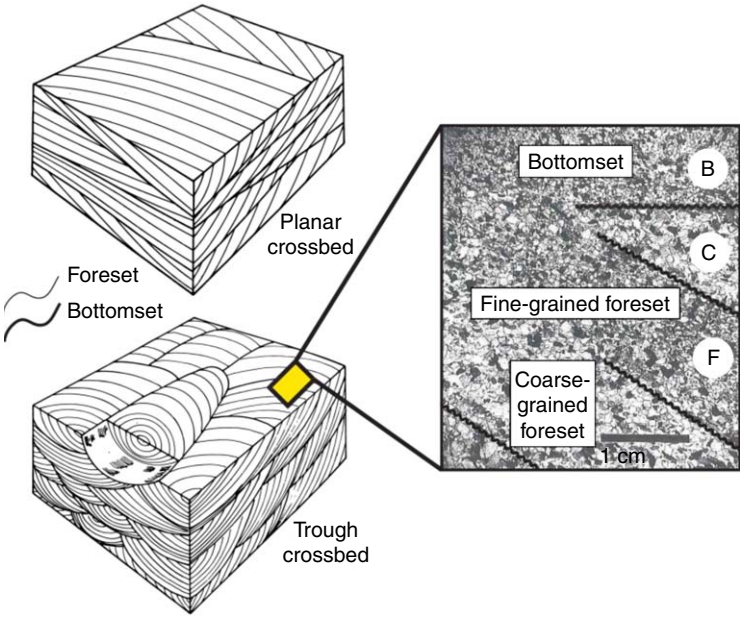

Fig. 2—Left: Two common varieties of cross stratification (Reineck and Singh 1980). Right: Changes in grain-size distribution across consecutive laminae as seen in a crossbed thin section from a fluvial outcrop (Hartkamp-Bakker 1993).

Falls et al. (1988) observed foam generation and mobilization experimentally in a bead pack with a permeability contrast of approximately 20:1. They also experimentally measured a critical capillary pressure for snap-off (P_c^{sn}) for the bead packs used and found it to be approximately half the capillary entry pressure of the medium. For snap-off to occur, enough liquid must accumulate in the low-permeability section to cause the capillary pressure to drop below P_c^{sn}. Rossen (1999) uses this finding and a pore-network model to illustrate that for snap-off to occur at the boundary between two homogeneous regions differing in permeability, the minimum permeability ratio required is 4. A higher permeability contrast is required for drier flow. Once again, it is important to note that there is no pressure-gradient criterion for the creation of foam through this mechanism, though there might be such a condition for the mobilization of the foam. Tanzil et al. (2002) report visual observations of foam generation and mobilization across such a sharp transition in

permeability in their coreflood experiments with sandpacks inside a transparent glass column. They used a permeability ratio of 4.4:1 and an injected-gas fraction of 67% for their experiments. Their experimental procedure, however, began with coinjection of gas and surfactant solution into a medium already saturated with surfactant solution, representing a drainage process. As discussed above, other mechanisms of foam generation (Roof snap-off and leave-behind) contribute toward the observed gas-mobility reduction during drainage. Contrary to the findings of Tanzil et al. (2002), Li and Rossen (2005) did not observe foam generation in their sandpack experiments with permeability contrasts of 4.3:1 and 5.1:1. Their experiment started with coinjection of gas and brine into a brine-saturated medium, followed by coinjection of gas and surfactant solution once steady state had been reached. They suspected that gas bypass along the edges of the pack because of imperfect packing might have been the reason for failing to observe foam generation. They did, however, report foam generation during flow across a much greater permeability contrast of 20:1. The mobilization of this foam was periodic.

In this work, we follow an experimental procedure similar to the work of Li and Rossen (2005) and use a consolidated porous medium to examine the process of foam generation across an abrupt permeability jump. The main objective of this work is to validate the theoretical predictions of foam generation (Rossen 1999) through coreflood experiments that isolate snap-off resulting from a capillary pressure contrast as the only lamella-creation mechanism. We follow field-like superficial velocities to replicate the driving force encountered far from wells in a subsurface reservoir. We measure pressure gradient across several sections of the core to accurately identify the location for the first onset of foam generation and also to observe the propagation of this foam downstream. The experiments are assisted by X-ray CT to help visualize phase saturations as foam is generated and subsequent propagation commences.

This paper is structured as follows. The Experimental Design section describes the experimental setup, the porous media used, and the procedure followed in the experiments reported. The Results section reports the results of the foam-generation experiments with pressure and CT data obtained through the course of the experiment. The Discussion section provides the analysis of experimental results, and is followed by the Conclusions section.

Experimental Design

Materials and Chemicals. We perform coreflooding experiments with coinjection of gas and surfactant solution into an artificial porous medium made from sintered borosilicate glass. The cores were acquired from a commercial supplier and were prepared by sintering crushed, pure borosilicate glass. Each core had a single sharp jump in permeability roughly one-third of the way into the length of the core. In other words, roughly one-third of the core comprised a homogeneous low-permeability section whereas the rest of the core was made of a homogeneous high-permeability porous medium. The permeability change is achieved by sintering different grain sizes in the same core. The glass grains are angular as can be seen in the picture on the right in **Fig. 3.** While the cores were homogeneous in the axial direction, this was not always the case in the radial direction. On average, the porosity of the medium was 2 to 3% higher in a region roughly the size of a grain (≈0.1 to 0.5 mm for the cores used in this work) at the edges of the cylindrical core, compared with the bulk. This imperfection could be a result of differential expansion and contraction during the heating-up and cooling-down phase of the sintering process. Therefore, in the early stages of each experiment (described below), a significant amount of gas bypassed the brine-saturated core through the edge of the pack. Li and Rossen (2005) contend that this flow along the edges caused them to observe no foam generation across permeability contrasts of 4.3:1 and 5.1:1. However, this did not appear to affect our experiments, as we still observed foam generation across similar permeability contrasts as reported in the Discussion section.

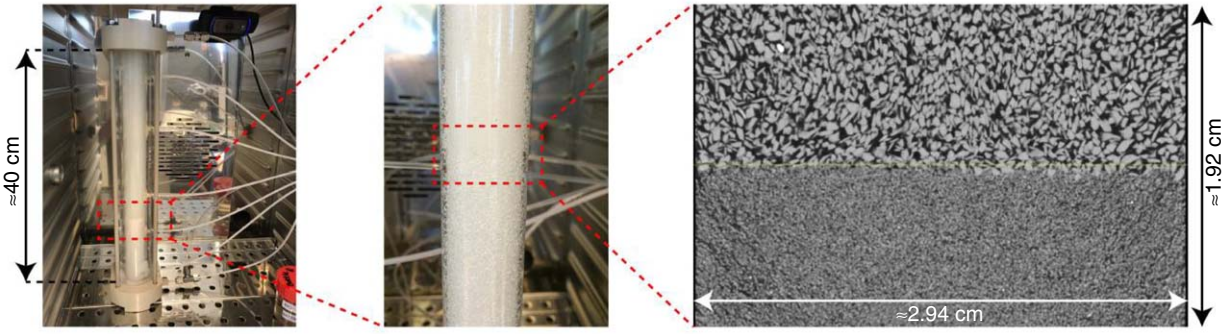

Fig. 3—Left: Core holder, (left and center) with sintered-glass core. Right: a μCT image (with a voxel size of 30 μm) of a vertical cross section across the permeability change.

The cores were prepared in a glass tube with an internal diameter of 3 ± 0.1 cm and were cut after the sintering process to roughly 40 ± 2 cm in length. The core was enclosed in acrylic glass with polyether-ether-ketone end caps. Four different core samples with different permeability ratios were acquired from the manufacturer, the details of which are given in **Table 1.** The permeability to water is determined from the slope of the straight line formed by a plot of superficial velocity vs. the ratio of pressure gradient measured across the two core sections to viscosity (i.e. q/A vs. $\nabla P/\mu$). The confidence interval for estimating this slope is also reported in darcies.

Anionic alpha olefin sulfonate (AOS) $C_{14–16}$ with a molecular weight of 315 g/mol was used as a foamer at an active concentration of 0.5 wt% (≈0.04 M). The surfactant solution was prepared using demineralized water also containing 1 wt% (≈0.17 M) NaCl. The critical micelle concentration (CMC) of this surfactant in demineralized water with 1 wt% NaCl was measured by Kahrobaei et al. (2017) using the Du Noüy ring method and reported to be 0.008 wt%. Therefore, the experiments presented in this paper are conducted at roughly 62 times the CMC. The properties of foam films stabilized by this surfactant in the presence of NaCl as an electrolyte are described by Farajzadeh et al. (2008). Nitrogen (N_2) with a purity of 99.98% was used as the gas phase in our experiments.

Experimental Apparatus. A schematic flow diagram of the experimental setup is shown in **Fig. 4.** The core is held horizontal in order to minimize the impact of beam-hardening effects and cross-artifacts while taking CT scans. Pressure gradient is measured every second across several sections of the core. In the low-permeability section, pressure gradient is used to confirm that there is no foam present or being generated as the experiment begins. Across the permeability transition, pressure gradient indicates whether there is any

foam being generated at the face of the heterogeneity. In the high-permeability section, pressure drop is used to monitor the mobilization of foam generated at the permeability change. We avoid the use of backpressure regulators and use atmospheric backpressure instead, to avoid fluctuations introduced by multiphase flow through the backpressure regulator. Any fluctuation in pressure at the downstream end could travel upstream, causing local fluctuations that would assist in foam generation. Therefore, the outlet of the core is open to atmosphere. The entire apparatus is placed on top of the CT scanner table. The medical CT scanner is housed in a temperature-controlled room at 21 ± 0.4°C.

Core Sample	Pore Size (specified by manufacturer)	Approximate Pore Volume (mL)	Permeability	k^H/k^L
1	Low perm: 16–40 μm High perm: 40–100 μm	99	Low perm (k^L): 5.4±0.02 darcies High perm (k^H): 20.7±0.2 darcies	3.8
2	Low perm: 40–60 μm High perm: 100–160 μm	99	Low perm: 10.9±0.01 darcies High perm: 59.3±0.8 darcies	5.4
3	Low perm: 16–40 μm High perm: 100–160 μm	80	Low perm: 3.1±0.01 darcies High perm: 43.2±0.2 darcies	13.9
4	Low perm: 16–40 μm High perm: 100–160 μm	96	Low perm: 1.7±0.15 darcies High perm: 46.7±2.0 darcies	27.5

Table 1—Absolute permeability of individual sections and corresponding permeability contrast in heterogeneous sintered-glass core samples used in the experiments.

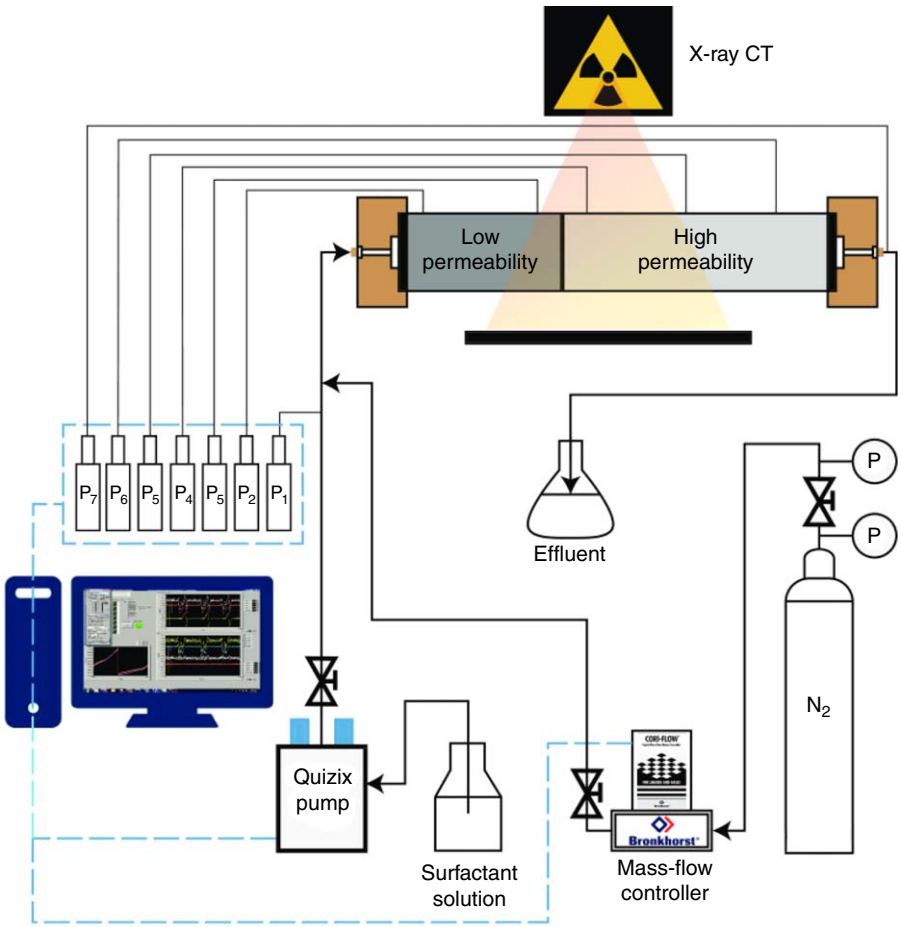

Fig. 4—Schematic of the experimental apparatus.

A dual-energy CT scanner was used in this study. Because the experiments involved two-phase flow of fluids differing greatly in density, a single energy X-ray beam was used to scan the core. An overview of the image settings used is reported in **Table 2.** Single-slice helical CT scans were acquired with a pitch of 0.9, resulting in approximately 260 slices in each scan along the axis of a core, taken over a period of approximately 9 seconds for each core. A pitch less than 1.0 ensures X-ray beam overlap for the same scanned volume, resulting in a better image quality. One slice contains 512 × 512 pixels, a part of which contains the circular core cross section. The images obtained were further processed to compute phase saturations using Fiji (Schindelin et al. 2012), a distribution of ImageJ software.

Parameter	Setting
Tube voltage	140 keV
Tube current	250 mA
Pitch	0.9
Slice thickness	1.5 mm
Pixel size	1.5×1.5 mm^2
Scan mode	Spiral

Table 2—CT-scan settings.

Experimental Procedure. The basic sequence of steps carried out through each coreflooding experiment is as follows.

Permeability Measurement. The setup is checked for leaks every time a new core is placed inside the core holder. Following the leak test, CO_2 is injected into the core for approximately 10 pore volumes (PVs) to displace air present in the core. The last 2 PV of CO_2 are injected under vacuum. While under vacuum, demineralized, degassed water is injected at low flow rates of approximately 10^{-3} PV/min into the core to displace the CO_2. After water breakthrough, the core is brought to atmospheric pressure by closing the outlet and continuing water injection. Water injection is continued for one more PV, following which the permeability of the core is measured by measuring pressure drop across different sections of the core at different flow rates. Next, the core is flushed with 1 wt% NaCl brine and the permeability is recalculated. Measured permeability is used as the first indicator for the presence of any trapped gas in the core, especially when conducting multiple experiments with the same core.

Foam-Generation Experiment. At the end of the permeability measurement, the core is fully saturated with brine. To start the experiment, brine-flow rate is set to the desired value and gas is introduced at the required fractional flow. Once gas-brine injection has reached steady state, brine injection is replaced by surfactant injection. This procedure ensures that no foam is generated under drainage conditions. During the course of the experiment, we expect to see foam generation in the core. Once the experiment has reached steady state or sufficient data have been acquired, injection is stopped and the core-cleaning procedure commences.

Core-Cleaning Procedure. After each experiment, the core is flushed with approximately 10 PV of 50 wt% isopropanol solution to kill the foam. This is followed by approximately 10 PV of demineralized water injection to remove all the alcohol and remaining surfactant solution from the system. If more experiments are to be performed with the same core, this step is followed by CO_2 injection and the permeability-measurement protocol.

Results

Foam generation was observed in each experiment performed. All the experiments reported in this paper were carried out at a total injection rate (q_t) of 0.1 mL/min and a gas fractional flow of 80%. On average, this translates to approximately 1.4 PV/D of total fluid injection for each core, which corresponds to a superficial (Darcy) velocity of 2.36 μm/s (0.67 ft/D) for each core. This superficial velocity was selected on the basis of observations from a series of tests conducted at different flow rates. The objective of these tests was to select a velocity that was low enough to cause foam generation across the permeability transition only, registered by a pressure greater than the accuracy of the transducers, and in an experiment completed within a reasonable time frame. The "incubation effect" reported by Baghdikian and Handy (1991) and more recently observed by Kahrobaei et al. (2017) could result in foam generation throughout the core when injection of surfactant solution and gas continues for long periods of time equivalent to several tens of PV. At a velocity of 3.34 ft/D (0.5 mL/min), foam generation was observed in the inlet low-permeability section itself; evidently, the pressure gradient in the low-permeability section was higher than the minimum pressure gradient required for foam generation. At a velocity of 1.34 ft/D (0.2 mL/min), foam generation was observed across the permeability transition and not in the inlet section. However, this total superficial velocity was still higher than that for fields with larger well spacing, as is often the case in offshore developments. At a superficial velocity of 0.67 ft/D (0.1 mL/min), we observed foam generation across the permeability jump and no foam in the inlet section, at least at the onset of foam generation across the heterogeneity. At flow rates lower than this, the experiment would take several weeks to conclude and the fluid velocities through the core would no longer be representative of conventional reservoir flow. Therefore, we selected a total superficial velocity of 0.67 ft/D for all subsequent experiments. Injected-gas fraction was fixed at 80% in order to align with the theoretical predictions of Rossen (1999), who showed that snap-off in flow across an abrupt permeability increase depends on both gas fractional flow and permeability contrast. In his model, for foam generation to be observed at 80% gas fractional flow, the permeability contrast must be 4:1 or higher. Conversely, in flow across a permeability contrast of 4:1, the gas fractional flow must be 80% or lower in order to see foam generation. With the objective of validating this threshold in mind, because the lowest permeability contrast considered in this study was close to 4:1, an injected-gas volume fraction of 80% was selected. In order to maintain consistency while studying the effect of permeability contrast, fractional flow was fixed at this value for all experiments.

Core 1. A foam-generation experiment was conducted with Core 1, which has a permeability contrast of 3.8:1, very close to the theoretical prediction of 4 required to cause foam generation by snap-off at 80% gas fractional flow (Rossen 1999). **Fig. 5** shows the measured absolute pressures and the corresponding pressure gradient across various sections of the core. The origin of the plot represents the start of surfactant injection into the core, after steady state has been achieved for the coinjection of gas and brine. Absolute pressure is measured at seven locations across the length of the core, schematically shown in Fig. 4. The pressure transducers are connected to the top of the horizontally placed glass core. In the bottom plot of Fig. 5, pressure gradient across four sections of the core is plotted: The inlet and outlet sections are ignored for the sake of readability.

Following Fig. 5, pressure gradient across the permeability transition rises sharply soon after gas is introduced into the core at 80% volume fraction. As coinjection of gas and brine reaches steady state, ∇P_2^{LH} continues to register an unusually high pressure gradient. We believe that this is because of pressure taps across the permeability transition sensing different phases (McCool et al. 1983; Chen et al. 2016). This is further aggravated by gas trapping and the capillary effect caused by a sharp difference in capillary pressure between the two zones in this section. After surfactant injection begins, the measured pressure gradient shows a mild and gradual drop from approximately 0.3 PV to 1.0 PV of total injection. We suspect that this is because of a diffused surfactant front reducing the interfacial tension (IFT) and, subsequently, the capillary pressure between the two phases at the pressure tap. It could also be because of a

gradual buildup in gas saturation near the pressure tap in the high-permeability zone (McCool et al. 1983). In bulk, an increase in surfactant concentration reduces IFT only below the CMC. At concentrations beyond the CMC, surfactant concentration has negligible effect on IFT. Therefore, only a small amount of surfactant solution at a concentration much higher than its CMC would be enough to dramatically reduce surface tension and capillary pressure.

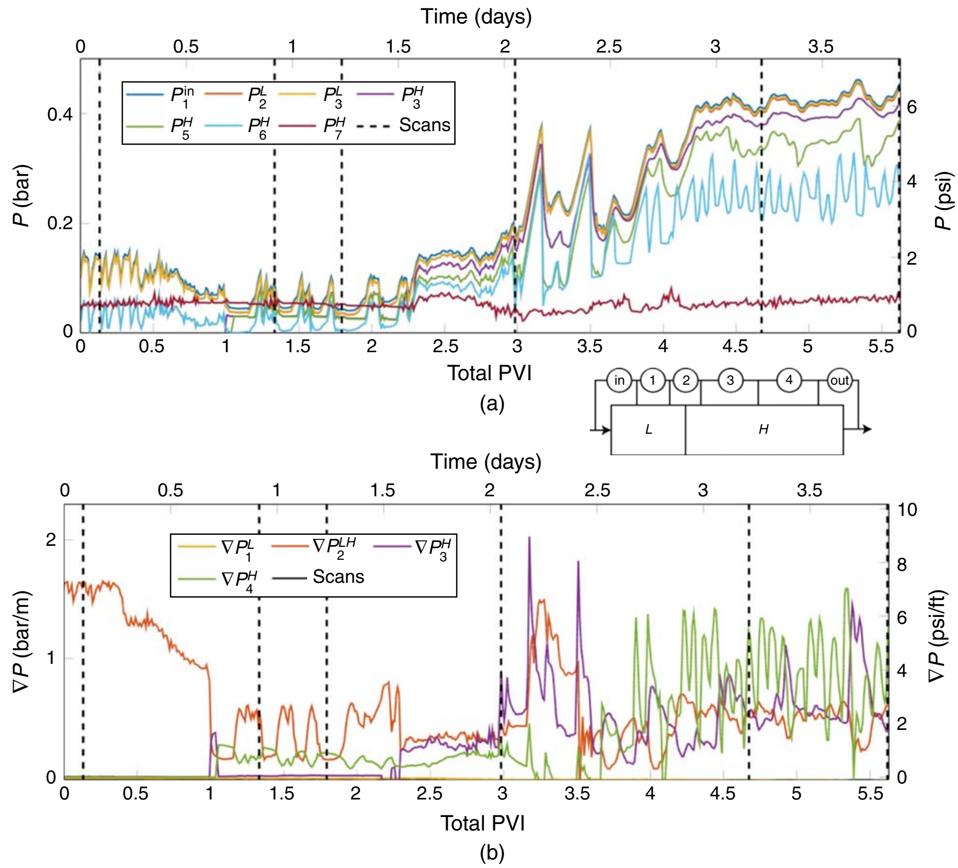

Fig. 5—(a) Absolute pressure and (b) pressure gradient across various sections of Core 1 during foam-generation experiment. Dashed lines indicate times at which CT scans were taken to generate saturation maps across the length of the core. Superscript L represents a measurement in the low-permeability section, while superscript H represents data acquired from the high-permeability zone. LH represents the interval with the boundary.

Pressure gradient ∇P_1^L across the low-permeability zone is negligible through the course of the experiment, which suggests that there is no significant reduction in mobility or indication of strong foam present or being generated in the inlet section of the core. Dashed lines in Fig. 5 indicate times at which CT scans were taken across the entire length of the core. Raw CT data in terms of Hounsfield units are used to compute porosity and phase saturations as a voxel property for each image stack. Porosity can be obtained using the CT scans of a dry core and a water-saturated core (Mees et al. 2003). During the course of the experiment, liquid-phase saturation is computed for each scan as

$$S_{\text{liq}} = \frac{CT_{\text{exp}} - CT_{\text{dry}}}{CT_{\text{liq}} - CT_{\text{dry}}}, \quad (1)$$

where CT_{exp} denotes the CT measurement taken during the course of the multiphase-flow experiment. CT_{dry} is the CT measurement of a dry core, obtained when the core is not yet saturated with any liquid, before each experiment. CT_{liq} represents the CT measurement for a core that is fully saturated with the liquid whose saturation is being computed. It is important to note that the accuracy of CT measurements depends on different parameters selected for the X-ray source, such as applied beam voltage, corresponding beam energy, and the applied filters for shaping the beam. **Fig. 6** shows the liquid-phase saturation in the core computed using Eq. 1. The saturation is shown across a vertical cross section through the center of the core during different stages of the experiment. The pixel size in each image slice is $195 \times 195\ \mu\text{m}^2$, and each slice is 1.5 mm thick. Liquid-phase saturation values are averaged in each cylindrical slice and plotted across the core length in **Fig. 7.** Note that while reporting CT measurements in this paper, a distance of approximately 2 cm from the entrance and exit face has been cropped from the CT images of each core. This is done in order to avoid any misinterpretation stemming from the entrance and end effects associated with corefloods. Moreover, anomalies in the saturation profile could arise from the first centimeter of each end of the core residing in the end cap whereas the rest of the porous medium is only surrounded by the glass tube that houses it, as can be seen in Fig. 3.

When gas and brine are injected into the core, most of the gas overrides to the top and bypasses a large part of the core, as can be seen in the saturation map at the top in Fig. 6. Once surfactant is introduced into the core, it appears that there is a buildup in gas saturation suggesting that foam is perhaps being generated in the first section itself, as can be seen in the CT image at 0.03 PV of liquid injected (0.13 total PVI). This is most likely a very weak foam because it is not persistent and is absent in the images thereafter. Moreover, there is no significant rise in ∇P_1^L (Fig. 5) to demonstrate mobility reduction and the presence of foam downstream of the inlet. After 0.4 PV of surfactant injection (1.8 total PVI), a modest reduction in gas mobility is recorded in the section with the permeability

transition (Fig. 5). This shows up as a higher gas-phase saturation just at the entrance of the high-permeability zone, clearly discernable in Fig. 7. At roughly 2.3 PVI, pressure gradient downstream of the permeability jump, ∇P_3^H and ∇P_4^H, begins to rise (Fig. 5) indicating a reduction in gas mobility as a result of foam propagation. This is verified by the CT response, which shows a foam front propagating through the high-permeability zone at 0.6 PVI of liquid (3.0 total PVI). At 0.9 PVI of liquid, CT images show that the foam front has reached the outlet of the pack and there is still no foam in the low-permeability zone. This gives a clear indication of foam generation at the sharp permeability increase and subsequent propagation downstream toward the outlet of the core.

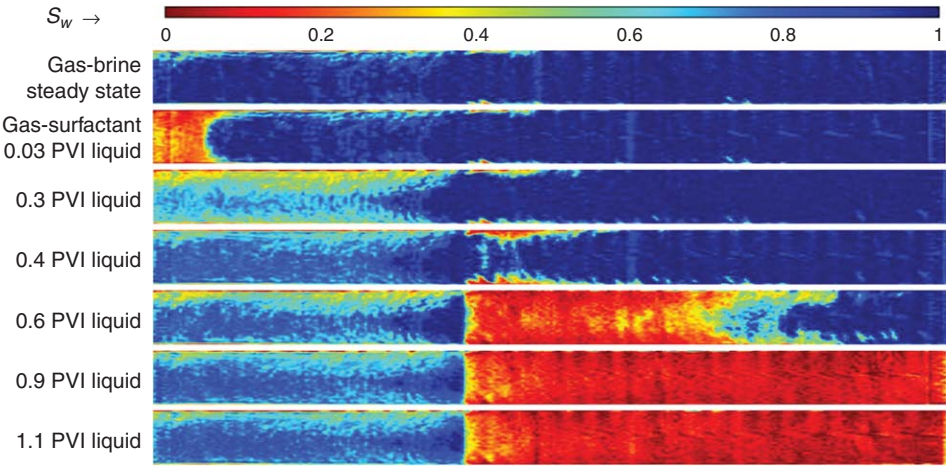

Fig. 6—Average liquid-saturation profile computed using X-ray CT imaging as seen in a vertical cross section through the center of Core 1. Color bar represents a liquid saturation range from 0 to 1. A high liquid-phase saturation is represented by blue, whereas red represents a high gas saturation, here interpreted as the CT response to the saturation change caused by foam. Top-most saturation map comes from the CT image taken during gas-brine injection and images thereafter were taken after surfactant solution was introduced in the core.

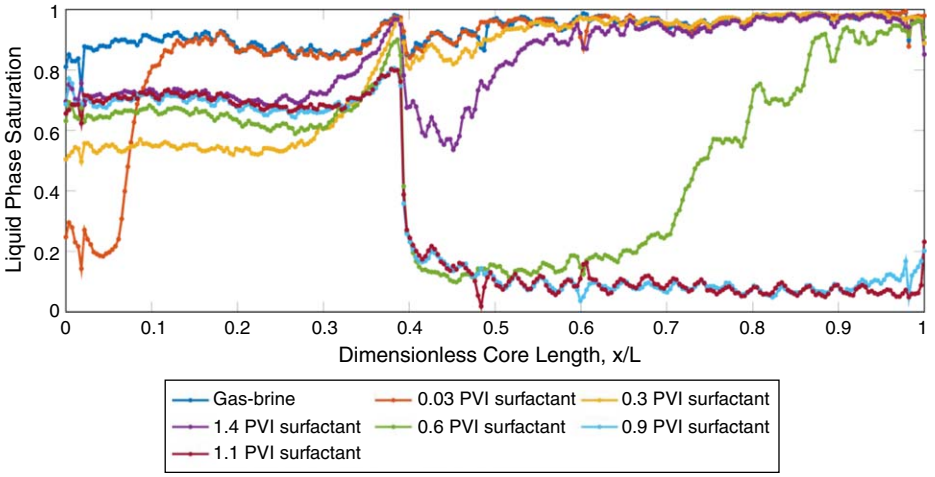

Fig. 7—Average liquid-phase-saturation profile in Core 1 at different PVs of injection (PVI) through the course of the foam-generation experiments in Fig. 6.

Core 2. A foam-generation experiment was performed in Core Sample 2, with a permeability contrast of 5.4:1 between the low- and high-permeability zones. The pressure gradient across different sections of the core developed with time in a manner similar to that in Sample 1, as shown in **Fig. 8.**

Once again, the pressure gradient across the permeability change gradually declines after surfactant is introduced in the core. There is a sharp drop in ∇P_2^{LH} and a sharp jump in the downstream pressure gradient ∇P_3^H at approximately 1.7 total PVI. As shown in **Fig. 9,** CT images at 0.4 PVI of surfactant solution (1.9 total PVI) show that this coincides with an increase in gas saturation in the high-permeability zone. The images also suggest that the preferred path of gas flow is along the edges of the core, which means that the initial onset of foam generation takes place right at the entrance to the high-permeability zone near the walls of the core. This mobility reduction then forces the gas to flow through the center of the core, resulting in foam generation through the whole face of the heterogeneity.

Saturation values per cylindrical slice are plotted against the dimensionless core position in **Fig. 10.** The core is almost completely saturated with liquid during coinjection of gas and brine, because most of the gas breaks through from the edges of the core, more from the top than from the bottom. At 0.4 PVI of liquid, liquid saturation drops sharply at the entrance of the high-permeability zone, indicating foam generation. At 0.5 PVI of liquid, the foam front appears to have traveled from a dimensionless position of 0.6 to 0.9, roughly half the length of the high-permeability zone, into the fourth section of the core. This is also evident from the pressure-gradient profile

shown in Fig. 8 as ∇P_4^H begins to rise and exhibit sharp fluctuations, starting at approximately 2.1 PVI. At 0.7 PVI of liquid (3.5 total PVI), foam has propagated to the end of the pack and the gas saturation is approximately 90% in the high-permeability region. Gas saturation is roughly 20% in the low-permeability zone, and no significant reduction in mobility is witnessed in terms of pressure gradient (Fig. 8).

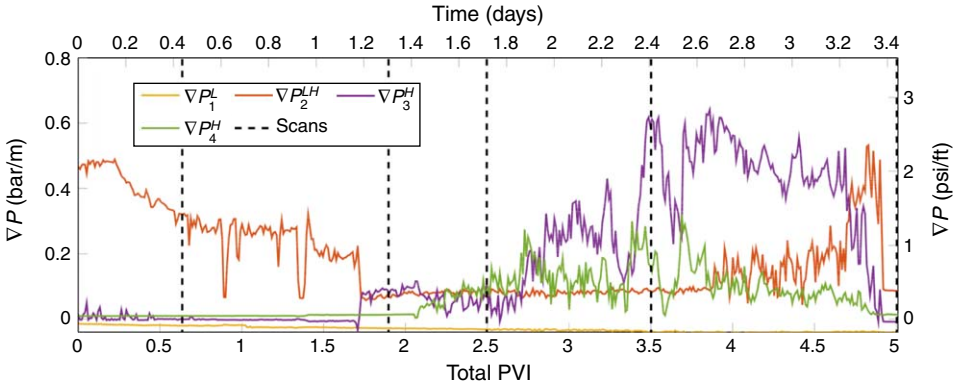

Fig. 8—Pressure gradient across various sections of Core 2 during foam-generation experiments. Dashed lines indicate times at which CT scans were taken to generate saturation maps across the length of the core. Superscripts L and H denote the low- and high-permeability sections, respectively. LH represents the interval with the boundary.

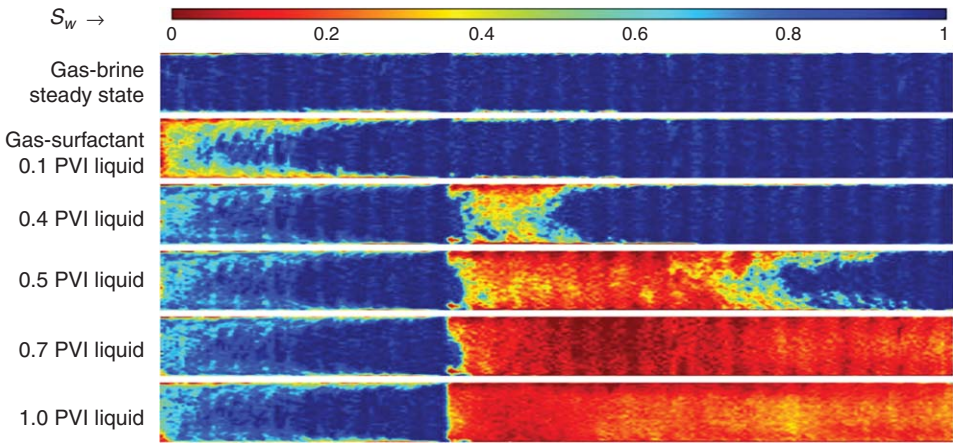

Fig. 9—Average liquid-saturation profile in a vertical cross section through the center of Core 2 computed using X-ray CT imaging during the course of a foam-generation experiment. Top-most saturation map comes from the CT scan taken during gas-brine injection, and images thereafter are from scans taken after surfactant solution was introduced in the core.

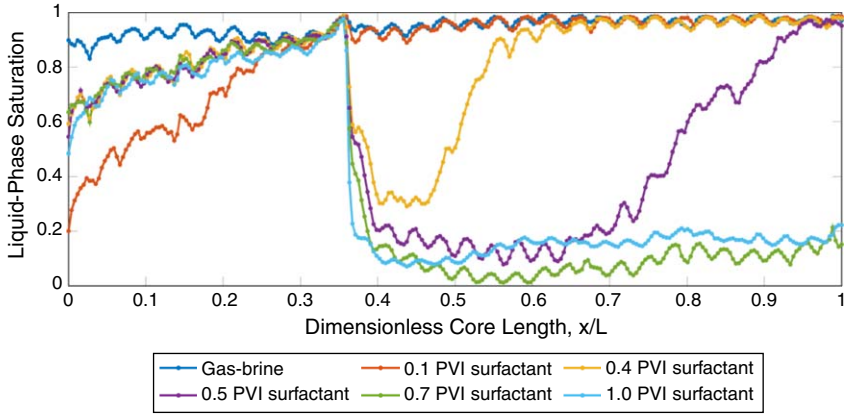

Fig. 10—Average liquid-phase saturation profile in Core 2 plotted at different PVI through the course of the foam-generation experiment.

Core 3. Foam generation was also observed in Core Sample 3, with a permeability contrast of 13.9:1. As shown in **Fig. 11,** pressure gradient across the permeability transition and further downstream showed distinct periods of rise and sharp drops, unlike the continuous and relatively mild fluctuating pattern observed in Fig. 5 and Fig. 8. The pressure gradient in the low-permeability section (∇P_1^L)

stays low through the course of the experiment, suggesting that there is no significant reduction in gas mobility. However, as shown in **Figs. 12 and 13,** the gas saturation is approximately 50% in the first section. This means that if there is any foam in the low-permeability section, it has little effect on gas mobility and is, therefore, weak foam. Evidently, even this weak foam transforms into strong foam at the permeability transition.

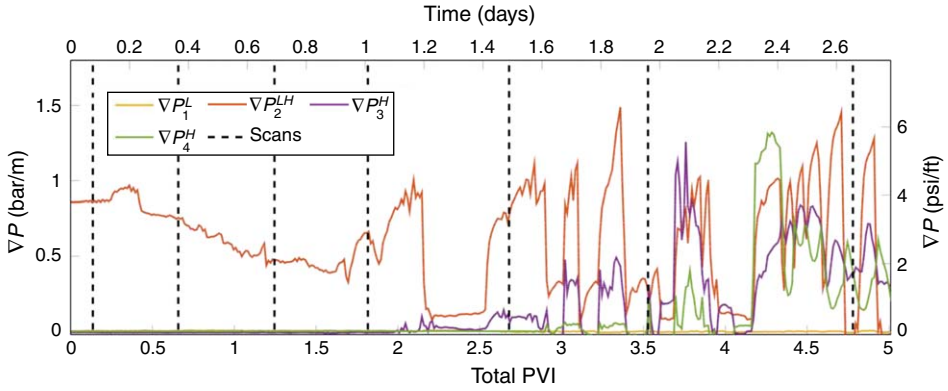

Fig. 11—Pressure gradient across various sections of Core 3 during foam-generation experiments. Dashed lines indicate times at which CT scans were taken to generate saturation maps across the length of the core. Superscripts L and H denote the low- and high-permeability sections, respectively. LH represents the interval with the boundary.

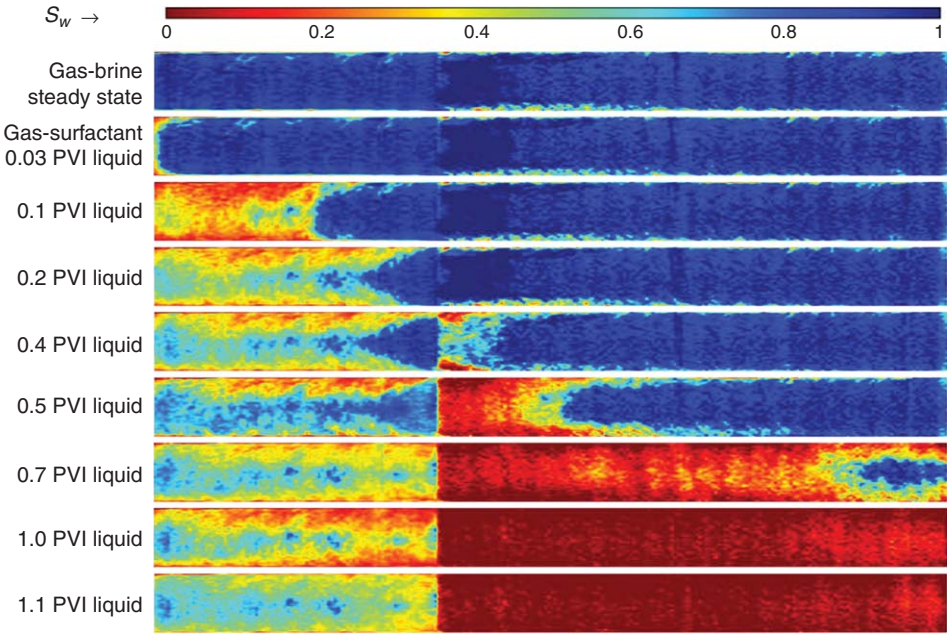

Fig. 12—Average liquid-saturation profile in a vertical cross section through the center of Core 3 computed using X-ray CT imaging during the course of a foam-generation experiment. Top-most saturation map comes from the CT scan taken during gas-brine injection, and images thereafter are from scans taken after surfactant solution was introduced in the core.

CT images in Fig. 12 also indicate that, as with Core Sample 2, there might be a region of high permeability along the edges of the core because of imperfect sintering of the glass grains with the tube wall. Gas prefers to flow along the edges of the core and foam generation also begins at the outer boundary of the cylindrical porous medium, shown clearly in the scan taken at 0.4 PVI of surfactant solution (Fig. 12). Images at 0.5 and 0.7 PVI of liquid (2.7 and 3.5 total PVI, respectively) show that the foam front propagates first along the edges, forcing gas to flow through the center of the porous medium, resulting in subsequent propagation of foam through the center of the core.

Core 4. Core Sample 4 had the greatest permeability contrast among the tested cores (27.5:1). We observe that strong foam is created across the permeability transition, and it propagates through the high-permeability zone to the end of the core. While the measured pressure gradient across the inlet section, as shown in **Fig. 14,** shows no appreciable increase indicating absence of strong foam, the saturation profile obtained through CT scans, as shown in **Fig. 15,** shows that the gas saturation is fairly high in the low-permeability zone toward the end of the experiment. Gas saturation is almost 70% in the low-permeability zone upstream of the transition as seen in the saturation profiles computed at 1.2 PVI of surfactant (6 total PVI) and thereafter. This rise in gas saturation, however, is witnessed only after foam generation across the transition has been observed. In the high-permeability section, CT images show a gas saturation of almost 100% toward the end of the experiment, indicating the presence of strong foam with a significant reduction in gas mobility, in terms of pressure gradient, as discussed in the next section.

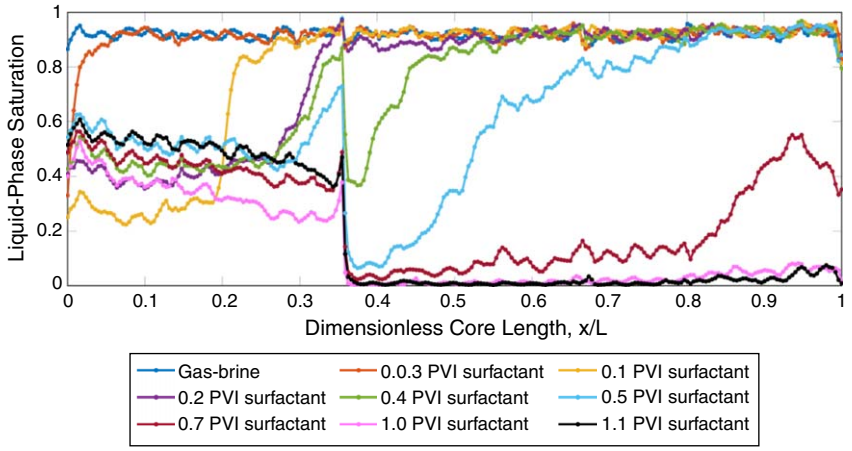

Fig. 13—Average liquid saturation vs. dimensionless core position during a foam-generation experiment in Core 3.

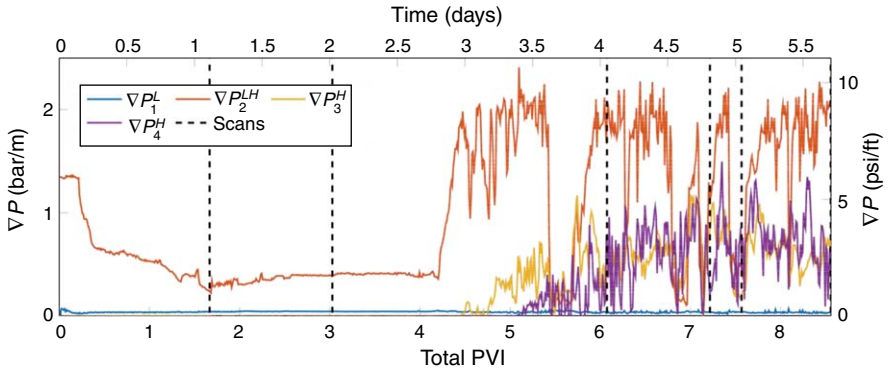

Fig. 14—Pressure gradient across variation sections of Core 4 during foam-generation experiments. Dashed lines indicate times at which CT scans were taken to generate saturation maps across the length of the core. Superscripts L and H denote the low- and high-permeability sections, respectively. LH represents the interval with the boundary.

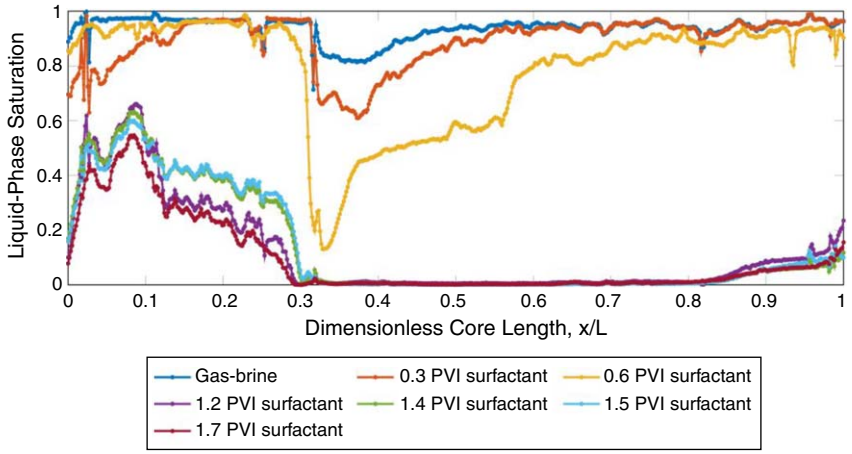

Fig. 15—Average liquid saturation vs. dimensionless core position during a foam-generation experiment in Core 4.

Discussion

In the experiments reported, we show evidence of foam generation across a sharp permeability rise during simultaneous flow of gas and surfactant solution. We observe foam generation across a permeability contrast of slightly less than 4:1 at a gas fractional flow of 80%, in accordance with theoretical predictions. While in some of our experiments we see indications of foam generation in terms of high gas saturation in the low-permeability section itself, this foam could be classified as "weak foam," or what Friedmann et al. (1991) call a "leave-behind foam," because gas mobility remains high (in terms of measured pressure gradient) in this section throughout the course of the experiment.

Foam generation does result in a significant reduction in gas mobility in the high-permeability zone. We quantify this reduction in mobility in terms of apparent foam viscosity. Assuming a steady-state average pressure drop across the high-permeability zone, we use the pressure gradient across the entire zone (Results section and herein) and compute apparent viscosity as

$$\mu_{\mathrm{app}} = \frac{k^H \nabla P}{u_l + u_g}, \quad (2)$$

where k^H is the measured permeability of the high-permeability zone, ∇P is the steady-state pressure gradient across the entire high-permeability zone measured after foam has propagated to the end of the core, and v_l and v_g are the superficial velocities of the liquid and gas phases, respectively. The apparent viscosity was averaged over quarter-day periods and plotted against total PVI in **Fig. 16.** Because the measurements are taken every second, there is a spread in the data collected and averaged over a 6-hour period. This spread is plotted in terms of an error bar in each direction, which represents one standard deviation of all the viscosities computed from all the recorded pressure gradients within the 6-hour measurement window.

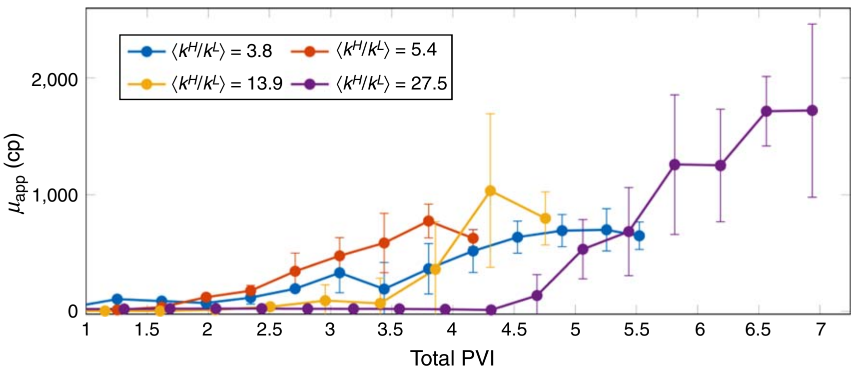

Fig. 16—Apparent viscosity of foam in the high-permeability region of each core, generated by flow across the abrupt permeability increase, plotted against the total PVI.

The average apparent viscosity of foam, generated across a sharp permeability increase, ranges from approximately 600 cp to 1,800 cp. Evidently, the greater the permeability contrast in the core, the larger the apparent viscosity of the generated foam. Additionally, we observe that at a greater permeability contrast, it takes longer to observe foam in the high-permeability section, especially in the core with the greatest permeability contrast, shown by the purple line in Fig. 16. We suspect that this may be a result of a greater intermittency in foam generation, as explained below, across greater permeability contrasts.

The measured pressure gradient in all our experiments exhibits large fluctuations. At a greater permeability contrast, the magnitude of these fluctuations is greater, as can be seen by the error bars in Fig. 16. These fluctuations occur because lamellae are not generated steadily across the face of the heterogeneity (Falls et al. 1988). Instead, foam generation across the sharp increase in permeability is intermittent. This can be explained as follows: Foam generation causes a reduction in gas mobility, which in turn causes the flow to become drier; locally, capillary pressure then rises above the critical capillary pressure for snap-off and foam generation ceases. After foam generation ceases, liquid accumulates again and the cycle repeats. This coincides with our observations at the outlet of the core. Distinct periods of liquid production were followed by strong foam coming out of the core, followed by relatively weaker and drier foam with a large bubble size, followed by periods of only gas production. The nature of produced fluids could also be affected by the capillary end effect at the outlet. In a separate set of experiments, we have observed that the intermittency of foam generation and subsequent mobilization are less frequent at a higher liquid fractional flow and a higher flow rate.

While designing the experiments reported in this paper, the objective was to create conditions for a uniform, 1D forced displacement across the permeability jump. However, as mentioned earlier, the porous medium was not perfectly homogeneous in the single-permeability regions and the unwanted artifact of imperfect sintering and higher porosity along the edges leads to preferential flow of gas near the walls of the core. While this might have resulted in unwanted experimental observations, complicating subsequent analysis, the aggravated effect of gravity (because of a low flow rate and high permeability) combined with this edge effect brought the experimental conditions closer to realistic geological settings. In a realistic subsurface setting, gas might have other flow paths available and may bypass the permeability boundary altogether, and not contribute to the process of foam generation. In the experiments presented in this paper, regardless of the availability of a preferential flow path for gas, foam generation was observed across the permeability jump. The experiments were designed so that foam was generated by snap-off and not because of drainage or a high pressure gradient. While Li and Rossen (2005) suggested that preferential flow along the edges of a core would make foam generation in such an experiment more difficult, this was not observed and snap-off still occurred at the permeability boundary at contrasts as low as 3.8:1 with a field-like total superficial velocity of 0.67 ft/D.

The results of this study can have important implications for the use of foam for mobility control in subsurface displacement processes. In a petroleum reservoir, 10 m away from the injection well, fluid velocity can be as much as 100 times lower than that in the immediate vicinity of the well. As a result, foam strength can be significantly lower and foam propagation might fail (Friedmann et al. 1994; Ashoori et al. 2012). However, quite often there exist sharp heterogeneities in the formation. When they are present, foam strength can still be maintained by snap-off across these permeability contrasts. If the impact of these heterogeneities on foam generation and propagation is not accounted for, the effectiveness of foam in reducing gas mobility can be underestimated. In order to understand the consequences of this phenomenon in a more realistic, or 3D, subsurface setting with layered or secondary granulometry, the results of this study could be used to model foam generation by snap-off in a flow across a sharp permeability change and the model could be used to simulate the displacement process in the analog system.

It is important to note that surfactant adsorption is negligible in our synthetic porous media made from borosilicate glass. Therefore, in our experiments, foam generation appears to be almost immediate once the surfactant arrives at the permeability transition. In the field, however, surfactant adsorption, whenever not satisfied, can delay the propagation of surfactant.

Conclusions

Simultaneous flow of gas and surfactant solution across a sharp permeability increase results in foam generation by snap-off, provided that the liquid volume fraction is high enough and permeability contrast is sufficient. Foam can be generated by this phenomenon at

extremely low superficial velocities, close to and even lower than conventional field velocities encountered far from wells. This coincides with theory, which suggests that this mechanism is independent of pressure gradient. CT images clearly indicate that foam is generated at the permeability change and that it propagates downstream toward the outlet of the core.

At the low flow rates used in these experiments, no effective foam was generated in the homogeneous core upstream of the permeability transition. Events of foam generation and subsequent mobilization are associated with sharp fluctuations in the pressure gradient across the permeability jump. Foam generation and propagation are not immediate as the surfactant front reaches the permeability jump. Instead, foam generates, propagates, and mobilizes intermittently from the permeability transition. The intermittency appears to be greater for greater permeability contrasts.

Foam generation during flow across abrupt permeability changes in the vertical direction could significantly reduce gravity segregation. Foam created during flow across layer boundaries would block the upward movement of gas toward higher layers. This would reduce the gas mobility in the vertical direction, effectively reducing vertical permeability to gas and increasing the segregation length (Jenkins 1984; Stone 1982; Tanzil et al. 2002; Rossen and van Duijn 2004).

Nomenclature

A = cross-sectional area of the core, m^2
CMC = critical micelle concentration, wt%
CT = X-ray CT measurement in Hounsfield units, HU
k = permeability, m^2
P = pressure, Pa
P_c = capillary pressure, Pa
∇P = pressure gradient, Pa/m
q = flow rate, mL/min
S = phase saturation, –
u = superficial (Darcy) velocity, m/s
μ = viscosity, cp

Superscripts

L = low-permeability region
LH = region with low- to high-permeability transition
H = high-permeability region
min = minimum, used to denote minimum ∇P or velocity required to generate foam
sn = snap-off, used to denote critical capillary pressure required for snap-off

Subscripts

app = apparent
dry = denotes CT measurement of the dry core
exp = denotes a CT measurement of the core during the foam-generation experiment
g = gas
l = liquid
liq = denotes CT measurement of the liquid-saturated core
t = total

Acknowledgments

This paper is a result of the collaboration between Delft University of Technology and Universiti Teknologi Petronas. We thank Petronas and Shell for funding this research. We gratefully acknowledge Michiel Slob, Ellen Meijvogel-de Koning, Marc Friebel, Karel Heller, and Joost van Meel for their extensive technical support at the Laboratory of Geoscience and Engineering of Delft University of Technology.

References

Ashoori, E., Marchesin, D., and Rossen, W. R. 2012. Multiple Foam States and Long-Distance Foam Propagation in Porous Media. *SPE J.* **17** (4): 1231–1245. SPE-15024-PA. https://doi.org/10.2118/154024-PA.

Baghdikian, S. Y. and Handy, L. L. 1991. Transient Behavior of Simultaneous Flow of Gas and Surfactant Solution in Consolidated Porous Media. USDOE Report DOE/BC/14600-10 (DE91002249). https://doi.org/10.2172/5434448.

Bernard, G. G. and Holm, L. W. 1964. Effect of Foam on Permeability of Porous Media to Gas. *SPE J.* **4** (3): 267–274. SPE-983-PA. https://doi.org/10.2118/983-PA.

Chang, J. and Yortsos, Y. C. 1992. Effect of Capillary Heterogeneity on Buckley-Leverett Displacement. *SPE Res Eval & Eng* **7** (2): 285–293. SPE-18798-PA. https://doi.org/10.2118/18798-PA.

Chen, X., Kianinejad, A., and DiCarlo, D. A. 2016. An Extended JBN Method of Determining Unsteady-State Two-Phase Relative Permeability. *Water Resources Research* **52** (10): 8374–8383. https://doi.org/10.1002/2016WR019204.

Falls, A. H., Hirasaki, G. J., Patzek, T. W. et al. 1988. Development of a Mechanistic Foam Simulator: The Population Balance and Generation by Snap-Off. *SPE Res Eval & Eng* **3** (3): 884–892. SPE-14961-PA. https://doi.org/10.2118/14961-PA.

Farajzadeh, R., Krastev, R., and Zitha, P. L. J. 2008. Foam Films Stabilized With Alpha Olefin Sulfonate (AOS). *Colloids and Surfaces A: Physicochemical and Engineering Aspects* **324** (1–3): 35–40. https://doi.org/10.1016/J.COLSURFA.2008.03.024.

Friedmann, F., Chen, W. H., and Gauglitz, P. A. 1991. Experimental and Simulation Study of High-Temperature Foam Displacement in Porous Media. *SPE Res Eval & Eng* **6** (1): 37–45. SPE-17357-PA. https://doi.org/10.2118/17357-PA.

Friedmann, F., Smith, M. E., and Guice, W. R. 1994. Steam-Foam Mechanistic Field Trial in the Midway-Sunset Field. *SPE Res Eval & Eng* **9** (4): 297–304. SPE-21780-PA. https://doi.org/10.2118/21780-PA.

Gauglitz, P. A., Friedmann, F., Kam, S. I. et al. 2002. Foam Generation in Homogeneous Porous Media. *Chemical Engineering Science* **57** (19): 4037–4052. https://doi.org/10.1016/S0009-2509(02)00340-8.

Hartkamp-Bakker, C. A. 1993. *Permeability Heterogeneity in Cross-Bedded Sandstones: Impact On Water/Oil Displacement in Fluvial Reservoirs*. PhD Dissertation, Delft University of Technology, Delft, Netherlands (September 1993).

Hirasaki, G. J., Jackson, R. E., Jin, M. et al. 2000. Field Demonstration of the Surfactant/Foam Process for Remediation of a Heterogeneous Aquifer Contaminated With DNAPL. In *NAPL Removal: Surfactants, Foams, and Microemulsions*, ed. S. Fiorenza, C. A. Miller, C. L. Oubre et al., 3–163. Boca Raton, Florida: CRC Press.

Huh, D. G. and Handy, L. L. 1989. Comparison of Steady and Unsteady-State Flow of Gas and Foaming Solution in Porous Media. *SPE Res Eval & Eng* **4** (1): 77–84. SPE-15078-PA. https://doi.org/10.2118/15078-PA.

Jenkins, M. K. 1984. An Analytical Model for Water/Gas Miscible Displacements. Presented at the SPE Enhanced Oil Recovery Symposium, Tulsa, Oklahoma, 15–18 April. SPE-12632-MS. https://doi.org/10.2118/12632-MS.

Kahrobaei, S., Vincent-Bonnieu, S., and Farajzadeh, R. 2017. Experimental Study of Hysteresis Behavior of Foam Generation in Porous Media. *Scientific Reports* **7:** 8986. https://doi.org/10.1038/s41598-017-09589-0.

Kam, S. I. 2008. Improved Mechanistic Foam Simulation With Foam Catastrophe Theory. *Colloids and Surfaces A: Physicochemical and Engineering Aspects* **318** (1–3): 62–77. https://doi.org/10.1016/j.colsurfa.2007.12.017.

Kovscek, A. R. and Radke, C. J. 1994. Fundamentals of Foam Transport in Porous Media. In *Foams: Fundamentals and Applications in the Petroleum Industry*, L. L. Schramm (Ed.), Chap. 3, 115–163. Washington, DC: American Chemical Society.

Li, Q. and Rossen, W. R. 2005. Injection Strategies for Foam Generation in Homogeneous and Layered Porous Media. Presented at the SPE Annual Technical Conference and Exhibition, Dallas, Texas, 9–12 October. SPE-96116-MS. https://doi.org/10.2118/96116-MS.

McCool, C. S., Parmeswar, R., and Willhite, G. P. 1983. Interpretation of Differential Pressure in Laboratory Surfactant/Polymer Displacements. *SPE J.* **23** (5): 791–803. SPE-10713-PA. https://doi.org/10.2118/10713-PA.

Mees, F., Swennen, R., Geet, M. Van. et al. 2003. Applications of X-Ray Computed Tomography in the Geosciences. *Geological Society of London, Special Publications* **215** (1): 1–6. https://doi.org/10.1144/GSL.SP.2003.21.

Ransohoff, T. C. and Radke, C. J. 1988. Mechanisms of Foam Generation in Glass-Bead Packs. *SPE Res Eval & Eng* **3** (2): 573–585. SPE-15441-PA. https://doi.org/10.2118/15441-PA.

Reineck, H. E. and Singh, J. B. (1980). *Depositional Sedimentary Environments*, second, revised and updated edition. Berlin: Springer Berlin Heidelberg. https://doi.org/10.1007/978-3-642-81498-3.

Rossen, W. R. 1996. Foams in Enhanced Oil Recovery. In *Foams: Theory, Measurements and Applications*, ed. R. K. Prud'homme and S. A. Khan, Chap. 11, 413–464. New York City: Marcel Dekker.

Rossen, W. R. 1999. Foam Generation at Layer Boundaries in Porous Media. *SPE J.* **4** (4): 409–412. SPE-59395-PA. https://doi.org/10.2118/59395-PA.

Rossen, W. R. 2003. A Critical Review of Roof Snap-Off as a Mechanism of Steady-State Foam Generation in Homogeneous Porous Media. *Colloids and Surfaces A: Physicochemical and Engineering Aspects* **225** (1–3): 1–24. https://doi.org/10.1016/S0927-7757(03)00309-1.

Rossen, W. R. and Gauglitz, P. A. 1990. Percolation Theory of Creation and Mobilization of Foams in Porous Media. *AIChE Journal* **36** (8): 1176–1188. https://doi.org/10.1002/aic.690360807.

Rossen, W. R. and van Duijn, C. J. 2004. Gravity Segregation in Steady-State Horizontal Flow in Homogeneous Reservoirs. *J Petr Sci Eng* **43** (1–2): 99–111. https://doi.org/10.1016/J.PETROL.2004.01.004.

Schindelin, J., Arganda-Carreras, I., Frise, E. et al. 2012. Fiji: An Open-Source Platform for Biological-Image Analysis. *Nature Methods* **9** (7): 676. https://doi.org/10.1038/nmeth.2019.

Stone, H. L. 1982. Vertical, Conformance in an Alternating Water-Miscible Gas Flood. Presented at the SPE Annual Technical Conference and Exhibition, New Orleans, Louisiana, 26–29 September.SPE-11130-MS. https://doi.org/10.2118/11130-MS.

Tanzil, D., Hirasaki, G. J., and Miller, C. A. 2002. Mobility of Foam in Heterogeneous Media: Flow Parallel and Perpendicular to Stratification. *SPE J.* **7** (2): 203–212. SPE-78601-PA. https://doi.org/10.2118/78601-PA.

van Lingen, P. P. 1998. *Quantification and Reduction of Capillary Entrapment in Cross-Laminated Oil Reservoirs*. PhD Dissertation, Delft University of Technology, Delft, Netherlands (October 1998).

van Lingen, P. P., Bruining, J., and van Kruijsdijk, C. P. J. W. 1996. Capillary Entrapment Caused by Small-Scale Wettability Heterogeneities. *SPE Res Eval & Eng* **11** (2): 93–99. SPE-30782-PA. https://doi.org/10.2118/30782-PA.

Yortsos, Y. C. and Chang, J. 1990. Capillary Effects in Steady-State Flow in Heterogeneous Cores. *Transport in Porous Media* **5** (4): 399–420. https://doi.org/10.1007/BF01141993.

Swej Shah is a PhD-degree candidate at the Department of Geoscience and Engineering, Delft University of Technology, The Netherlands. His current research interests include foam-generation mechanisms in porous media, population-balance models for modeling foam behavior, and multiscale methods for reservoir simulation. Shah holds a BS degree in chemical engineering from the Institute of Chemical Technology in Mumbai and an MS degree in applied Earth sciences from the Delft University of Technology. He is a recipient of the 2014 SPE Star Fellowship and winner of the 2016 SPE Europe student paper contest.

Karl-Heinz Wolf is associate professor in petrophysics at the Department of Geoscience and Engineering at Delft University of Technology. For 8 years, he was the director of the Geoscience and Engineering Laboratory and actively involved in CO_2-related EOR/enhanced-gas-recovery programs. Wolf works on the interfaces between geology, reservoir engineering, and geophysics, and develops petrophysical techniques for laboratory-scale rock-texture characterization/quantification. Also, his interests include clean coal technologies, in-situ oil (shale) combustion, and CO_2 enhanced coalbed methane. Many activities are linked to large experimental setups for scaled tests, as well as options to quantify images from outcrop to micro-CT-scan scale. Wolf is coauthor of more than 100 reviewed articles and research abstracts. He holds a PhD degree in applied Earth sciences from Delft University of Technology.

Rashidah Mohd Pilus is a senior lecturer and the deputy head of department at the Department of Petroleum Engineering at Universiti Teknologi Petronas, Malaysia. She holds a BS degree from the University of Nebraska, Omaha; an MS degree from McMaster University in Canada; and a PhD degree from Queen's University, Belfast, in Northern Ireland, all in chemistry.

William R. Rossen is professor of reservoir engineering at the Department of Geoscience and Engineering, Delft University of Technology. His current research concerns use of foams for diverting fluid flow in porous media, modeling complex transport processes in networks, and understanding flow in naturally fractured geological formations. Rossen was named Best Instructor at Delft University of Technology in 2011. In 2012, he was named an IOR Pioneer at the SPE/DOE Symposium on Improved Oil Recovery in Tulsa. Rossen is an SPE Distinguished Member.